J|A|C|S
ARTICLES

Published on Web 05/25/2010

Growth and Shape-Ordering of Iron Nanostructures on Au Single Crystalline Electrodes in an Ionic Liquid: A Paradigm of Magnetostatic Coupling

Yi-Min Wei,[†] Yong-Chun Fu,[†] Jia-Wei Yan,[†] Chun-Feng Sun,[†] Zhan Shi,[‡] Zhao-Xiong Xie,[†] De-Yin Wu,[†] and Bing-Wei Mao*,[†]

State Key Laboratory of Physical Chemistry of Solid Surfaces and Department of Chemistry, College of Chemistry and Chemical Engineering, and Department of Materials Science and Engineering, College of Materials, Xiamen University, 361005 Xiamen, China

Received March 15, 2010; E-mail: bwmao@xmu.edu.cn

Abstract: Fe electrodeposition on Au(111) and Au(100) in $BMIBF_4$ ionic liquid is found to form hitherto unreported shape-ordered nanoscale morphologies of pseudorods and pseudosquare rings, respectively, both composed of grains of 4−7 nm. The manner of growth of the square rings is a ring-on-ring structure with enlarging side length and slightly protruding four corners. The generality of the growth mechanism is verified by the formation of almost exactly the same shape-ordered Fe nanostructures on Pt, i.e., pseudorod structure on Pt(111) and pseudosquare rings Pt(100). These structures are explained within the framework of magnetostatic interactions of spontaneously magnetized grains under crystallographic constraint of the substrate surface, which result in an antiparallel arrangement in magnetization of the grains at pseudorods and magnetic flux closure at the pseudosquare rings. The closed magnetic flux further leads to magnetic field-enhanced growth at the four corners and the outer peripheries of the pseudosquare rings. The observed shape-ordering of the Fe thin film serves as a paradigm of magnetostatic coupling, in which the roles of ionic liquid as surfactant and magnetic media may not be underestimated. The present work adds a new dimension to electrodeposition in ionic liquid, by which new magnetic film structures may be expected.

1. Introduction

Supported ultrathin films of magnetic metals exhibit novel magnetisms which are strongly correlated with film structures as well as interactions with substrates.[1,2] Growth of the films with desired structures, and magnetism is of central concern toward deep understanding of nanomagnetism and future generation of magnetic devices. Fe is a typical magnetic element with special chemical properties. Its diverse applications in magnetic recording, chemical catalysis, and biomedical diagnoses have stimulated extensive investigations in the synthesis of Fe nanocrystals with tunable size and shape[3,4] and growth of Fe thin films via solution chemistry[5] and by electrodeposition[6] and vacuum deposition.[7−9] Electrodeposition benefits facile control of potential as well as variation of electrolyte composition including solvents and metal precursors.[10−12] So far, electrodeposition of ordered structures of Fe thin films has been mostly carried out in aqueous solutions using Au as substrates, and the main feature observed is the fcc to bcc phase transition as a result of strain release,[13,14] similar to that in UHV deposition.[15,16] One of the problems associated with electrodeposition of Fe in aqueous solutions is the hydrogen evolution reaction, which reduces the current efficiency and imposes severe H_2 bubble interference that could possibly alter the growth behavior. In this paper, we employ inert ionic liquid as solvent to show a paradigm change of nucleation/growth of Fe by electrodeposition.

Room-temperature ionic liquids have a wide electrochemical window and extremely low vapor pressure,[17,18] which have

[†] State Key Laboratory of Physical Chemistry of Solid Surfaces and Department of Chemistry.
[‡] Department of Materials Science and Engineering.

(1) Shiratsuchi, Y.; Yamamoto, M.; Bader, S. D. *Prog. Surf. Sci.* **2007**, *82*, 121.
(2) Vaz, C. A. F.; Bland, J. A. C.; Lauhoff, G. *Rep. Prog. Phys.* **2008**, *71*, 056501.
(3) Frey, N. A.; Peng, S.; Cheng, K.; Sun, S. H. *Chem. Soc. Rev.* **2009**, *38*, 2532.
(4) Park, J.; Joo, J.; Kwon, S. G.; Jang, Y.; Hyeon, T. *Angew. Chem., Int. Ed.* **2007**, *46*, 4630.
(5) Peng, S.; Wang, C.; Xie, J.; Sun, S. H. *J. Am. Chem. Soc.* **2006**, *128*, 10676.
(6) Chen, Y. X.; Chen, S. P.; Zhou, Z. Y.; Tian, N.; Jiang, Y. X.; Sun, S. G.; Ding, Y.; Wang, Z. L. *J. Am. Chem. Soc.* **2009**, *131*, 10860.
(7) Hwang, R. Q.; Bartelt, M. C. *Chem. Rev.* **1997**, *97*, 1063.
(8) Shen, J.; Ohresser, P.; Mohan, Ch. V.; Klaua, M.; Barthel, J.; Kirschner, J. *Phys. Rev. Lett.* **1998**, *80*, 1980.
(9) Li, J. L.; Jia, J. F.; Liang, X. J.; Liu, X.; Wang, J. Z.; Xue, Q. K.; Li, Z. Q.; Tse, J. S.; Zhang, Z. Y.; Zhang, S. B. *Phys. Rev. Lett.* **2002**, *88*, 066101.
(10) Kolb, D. M. *Angew. Chem., Int. Ed.* **2001**, *40*, 1162.
(11) Allongue, P.; Maroun, F. *J. Phys.: Condens. Matter* **2006**, *18*, S97.
(12) Möller, F. A.; Magnussen, O. M.; Behm, R. J. *Phys. Rev. Lett.* **1996**, *77*, 5249.
(13) Gundel, A.; Morrone, A.; Schmidt, J. E.; Cagnon, L.; Allongue, P. *J. Magn. Magn. Mater.* **2001**, *226*, 1616.
(14) Gundel, A.; Devolder, T.; Chappert, C.; Schmidt, J. E.; Cortes, R.; Allongue, P. *Phys. B* **2004**, *354*, 282.
(15) Stroscio, J. A.; Pierce, D. T.; Dragoset, R. A. *J. Vac. Sci. Technol. A, Vac. Surf. Films* **1991**, *10*, 1981.
(16) Voigtländer, B.; Meyer, G.; Amer, N. M. *Surf. Sci.* **1991**, *255*, L529.
(17) Galiński, M.; Lewandowski, A.; Stępniak, I. *Electrochem. Acta* **2006**, *51*, 5567.

10.1021/ja1021816

enabled electrodeposition of less precious ferromagnetic metals under flexible environmental conditions and with in situ scanning tunneling microscope (STM) characterization.[19−24] Furthermore, sufficient evidence has also indicated that the ions of ionic liquids can have strong interactions with electrode surfaces[25,26] or surfaces of as-formed nanoparticles.[27,28] Recently, Hamaguchi et al. have reported that the 1-butyl-3-methylimidazolium tetrachloroferrate (BMI[$FeCl_4$]) ionic liquid exhibits magnetic susceptibility due to possible local ordering of the magnetic anions $FeCl_4^-$.[29] These properties of ionic liquids could dramatically change the growth mechanism of magnetic metals and provide a possibility for growth of magnetic thin films with structures not achievable in aqueous solutions.

In this paper, we present an in situ STM study of Fe electrodeposition in 1-butyl-3-methylimidazolium tetrafluoroborate ($BMIBF_4$) ionic liquid using $FeCl_3$ as the precursor. Both Au(111) and Au(100) surfaces are employed to study the crystallographic influence on the morphology of the Fe thin film. We show that the growth of Fe in such a medium yields profound three-dimensional (3D) shape-ordered structures, which is attributed to magnetic coupling under magnetostatic interactions with crystallographic constraint. Our observations disclose a paradigm of magnetostatic coupling in the electrodeposition of ferromagnetic metals in ionic liquids by which new magnetic film structures may be expected.

2. Experimental Section

Synthesis of the $BMIBF_4$ ionic liquid has been described elsewhere.[30] $FeCl_3$ (Alfa, anhydrous, 98%) with a typical concentration of 0.05 M was used as the precursor because of its excellent solubility in $BMIBF_4$ and high chemical stability against O_2 oxidation. Prior to each STM and electrochemical measurement, the $FeCl_3$-containing $BMIBF_4$ was dried in vacuum at 70 °C for several hours to remove the absorbed water, and the experiments were conducted under the protection of N_2 atmosphere. The working surface was subjected to electrochemical polishing and flame annealing in H_2 followed by cooling under N_2 atmosphere. In situ STM measurements were carried out on Nanoscope E STM (Veeco, Santa Barbara, CA) under constant-current mode using mechanically cut PtIr tips, which were insulated by thermosetting polyethylene to reduce the Faradaic current. Platinum and Ag/AgCl wires were used as the counter and reference electrodes, respectively. Electrochemical experiments were performed on a CHI electrochemical workstation (Chenhua, Shanghai, China).

(18) Endres, F. *ChemPhysChem* **2002**, *3*, 144.
(19) Aravinda, C. L.; Freyland, W. *Chem. Commun.* **2004**, *23*, 2754.
(20) Lin, L. G.; Yan, J. W.; Wang, Y.; Fu, Y. C.; Mao, B. W. *J. Exp. Nanosci.* **2006**, *1*, 269.
(21) Mann, O.; Freyland, W. *J. Phys. Chem. C* **2007**, *111*, 9832.
(22) Wei, Y. M.; Zhou, X. S.; Wang, J. G.; Tang, J.; Mao, B. W.; Kolb, D. M. *Small* **2008**, *4*, 1355.
(23) Zhou, X. S.; Wei, Y. M.; Liu, L.; Chen, Z. B.; Tang, J.; Mao, B. W. *J. Am. Chem. Soc.* **2008**, *130*, 13228.
(24) Fu, Y. C.; Su, Y. Z.; Wu, D. Y.; Yan, J. W.; Xie, Z. X.; Mao, B. W. *J. Am. Chem. Soc.* **2009**, *131*, 14728.
(25) Lin, L. G.; Wang, Y.; Yan, J. W.; Yuan, Y. Z.; Xiang, J.; Mao, B. W. *Electrochem. Commun.* **2003**, *5*, 995.
(26) Su, Y. Z.; Fu, Y. C.; Yan, J. W.; Chen, Z. B.; Mao, B. W. *Angew. Chem., Int. Ed.* **2009**, *48*, 5148.
(27) Zhu, J. M.; Shen, Y. H.; Xie, A. J.; Qiu, L. G.; Zhang, Q.; Zhang, S. Y. *J. Phys. Chem. C* **2007**, *111*, 7629.
(28) Kramer, J.; Redel, E.; Thomann, R.; Janiak, C. *Organometallics* **2008**, *27*, 1976.
(29) Hayashi, S.; Hamaguchi, H. O. *Chem. Lett.* **2004**, *33*, 1590.
(30) Fu, Y. C.; Yan, J. W.; Wang, Y.; Tian, J. H.; Zhang, H. M.; Xie, Z. X.; Mao, B. W. *J. Phys. Chem. C* **2007**, *111*, 10467.

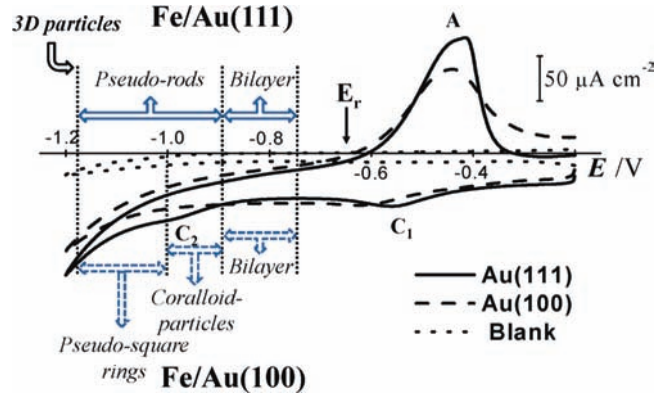

Figure 1. Cyclic voltammograms of Au(111) and Au(100) in ~50 mM $FeCl_3$ $BMIBF_4$ solution. Sweep rate: 50 mV s^{-1}.

3. Results and Discussion

Fe deposition occurs through discharge of the Fe(II) species that is generated from the reduction of the initially present Fe(III) precursor beginning at −0.2 V, but multispecies discharging is not excluded since $FeCl_4^-$ or $FeCl_4^{2-}$ species may be formed through solution chemistry. Cyclic voltammograms of electrodeposition of Fe are given by Figure 1. The equilibrium potential E_r for Fe bulk deposition is determined to be around −0.65 V, which is identified with the onset of the anodic current peak A associated with dissolution of the Fe deposit. The reduction of Fe(III) generates a considerable background current of ca. 25 $\mu A \cdot cm^{-2}$ on the CVs. The small and broad cathodic peak C_1 is associated with the adsorption of either $FeCl_3$ or $FeCl_2$.[22] Fe deposition appears kinetically hindered with a gradual increase of cathodic current upon cathodic potential sweep down to −1.2 V. The small cathodic wave C_2 at ca. −0.98 V is present only at Au(111).

Fe deposition is initiated by the formation of two-atom-high bilayer structures at lower overpotential. The bilayer on Au(111) is of fcc−Fe(111) structure with anisotropy along the three characteristic ⟨110⟩ directions of Au(111), resulting in short strips of about 4 nm in width and several to tens of nanometers in length. The bilayer on Au(100) is of bcc−Fe(100) structure with a rectangular feature along the two characteristic ⟨100⟩ directions of Au(100). Detailed STM images and proposed Fe bilayer structures are given in Figures 1S and 2S (Supporting Information).

The bilayer provides energetically more favorable sites for the follow-up 3D nucleation and growth at higher overpotential. On Au(111), nucleation of Fe occurs progressively and preferentially on top of the bilayer strips (see bright spots in Figure 2a,b). The initial nucleation process is accompanied by the formation of new bilayer strips. There is a probability that nuclei are initiated on the bare regions of the substrate surface, but we speculate that a bilayer has already formed underneath just upon the formation of such nuclei. As can be seen from Figure 2c, while nuclei increase in density and grow bigger, the size of the nuclei is almost restricted by that of the bilayer strips with reasonably uniform width of 4−6 nm. This leads to the formation of pseudorods following exactly the directions of the strips and with varying length of 20 ± 10 nm, Figure 2d. It is important to point out that the anisotropy of the pseudorods is maintained as Fe grows thicker, which reveals the necessity of the interlayer interaction between the adjacent Fe grains in the direction perpendicular to surface. Anisotropically grown Fe deposit on Au(111) has also been observed by Freyland and

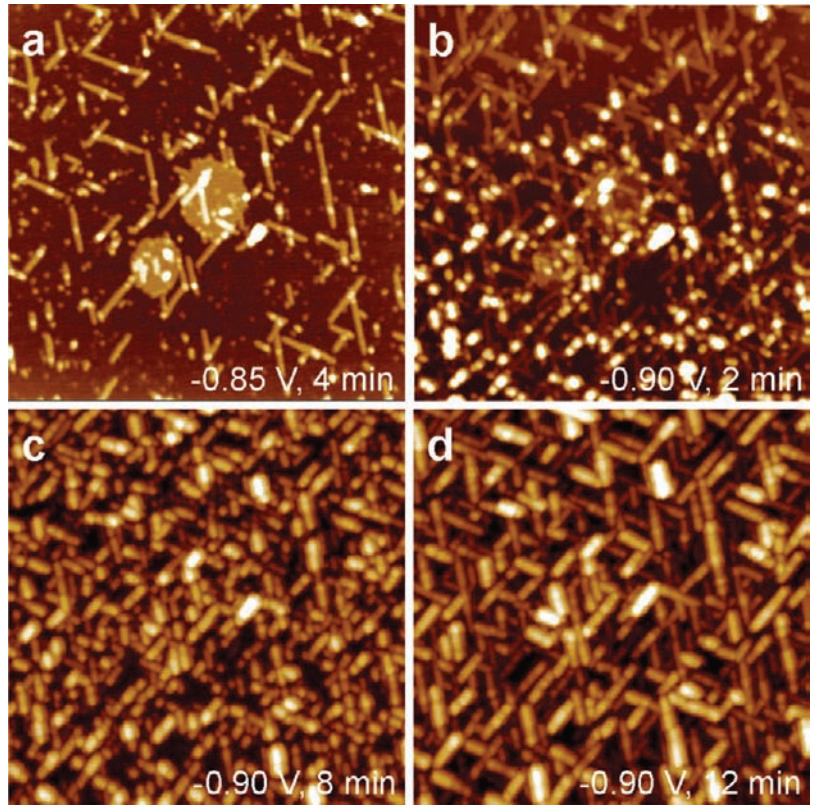

Figure 2. Sequence of STM images showing Fe nucleation and growth on Au(111): (a) preferential nucleation on the bilayer strips; (b) initial nucleation process is accompanied by the formation of new bilayer strips; (c, d) anisotropic growth to form 3D pseudorods which are composed of discrete grains. The time values given on the images are the time laps at the specified potentials. Scan size: 200 nm × 200 nm.

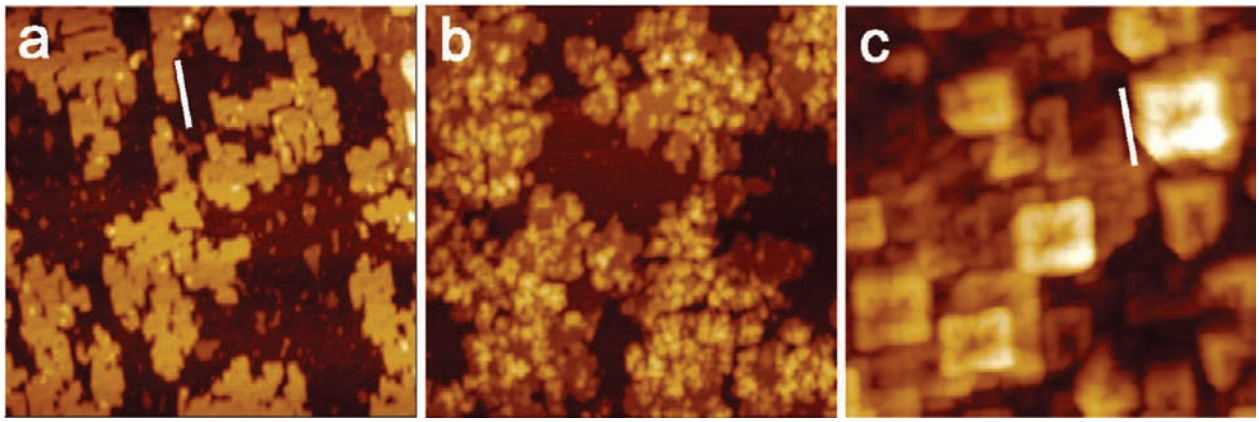

Figure 3. Fe nanostructures deposited on Au(100): (a) Fe bilayer formed at −0.85 V where small and sparsely distributed Fe nuclei already appear on top of the bilayer; (b) primary nucleation on top of the bilayer with formation of coralloid structure at −0.90 V; (c) pseudosquare rings grown in the secondary stage of nucleation at −1.10 V. The square rings are aligned with the characteristic directions of the Au(100) surface as indicated by the white lines in (a) and (c). Scan size: 100 nm × 100 nm.

co-workers in $\{AlCl_3-[MBIm]^+Cl^-\}$ ionic liquid,[19] but the size and details of their structure are very different from those of the pseudorods described here.

On Au(100), progressive and preferential nucleation also takes place on top of the incomplete bilayer, Figure 3a, as potential scans negatively to a critical potential around −0.85 V. A disordered film, composed of a coralloid structure with size of 2.5−4 nm is formed at slightly more cathodic potential of −0.9 V, Figure 3b, and we refer to the nucleation at this stage as primary nucleation. Details of the evolution of disordered film are given in Figure 4S (Supporting Information). The most intriguing feature of Fe deposition on Au(100) is the unusual secondary nucleation/growth taking place at more negative potential at −1.0 to −1.15 V. This process is characterized by a sudden emerging of small grains which develop into unique pseudosquare ring structures on the primary coralloid structure. Figure 3c shows the square rings grown to different sizes with average widths of 6−7 nm and various heights of 6−10 nm and side lengths of 10−30 nm. The square rings are also composed of small grains and have near 90° rectangle turnings with the four sides oriented along the ⟨100⟩ directions of the substrate. Depending on kinetic factors, these square rings may have different density, size, and even details of morphological features, but all of them have the common feature of right-angle turns; see Figure 5S (Supporting Information).

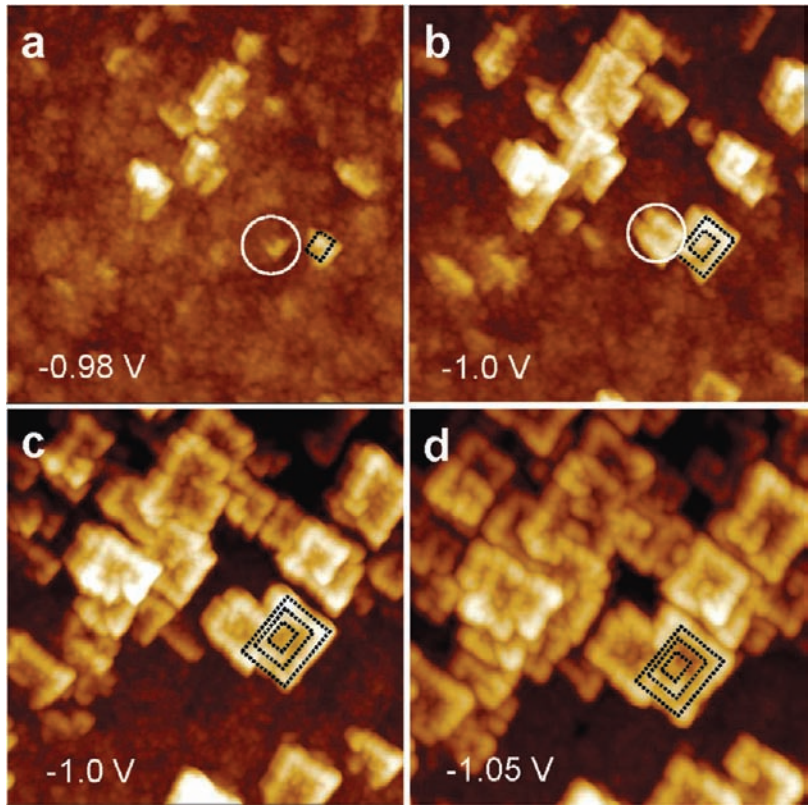

Figure 4. Evolution of the pseudosquare rings on Au(100). The nuclei are initiated at −0.98 V with at least one right angle turn (a) and develop into square rings (b). The rings expand outward and upward in a ring-on-ring manner (a−d). Potentials are indicated on the images, which were made slightly decreasing with time to promote faster growth for convenience of observation. The interval between (b) and (c) is 10 min. Scan size: 160 nm × 160 nm.

The evolution of individual pseudosquare rings can be followed by focusing on a region with less densely arranged nuclei. As shown in Figure 4a,b, nuclei with one or two right angles are initially formed (see the white circles), which develop further by turning at right angles to form pseudosquare rings. Further growth of the rings is characterized by expanding outward and upward in a ring-on-ring manner as indicated by the black dotted rectangles in Figure 4. Note that the four corners with right angle turnings are slightly protruding, implying enhanced growth at the corners. Furthermore, once the nuclei are formed in some areas, formation of new nuclei in the nearby surrounding areas seems to be inhibited until prolonged deposition or with application of larger overpotential.

The persistence of the orientation of the pseudorods on Au(111) and pseudosquare rings on Au(100) implies a three-dimensional ordering of the Fe deposit, which is otherwise challenging in the thin film growth. Furthermore, it is the unique pseudosquare rings, instead of cubes, that are formed on Au(100) in the secondary nucleation/growth stage. These features are hitherto unreported and far beyond the current understanding of metal deposition in electrochemical environment and in UHV. Therefore, unusual growth mechanisms have to be considered. Since Fe is a typical ferromagnetic element, elucidation of the mysterious growth mechanisms of the pseudorods and, in particular, of the pseudosquare rings should start by considering the magnetic properties of the Fe nanostructures. To facilitate further discussions, the proposed structures of 3D pseudorods and pseudosquare rings on the respective bilayers are illustrated in Figure 5.

First, for bcc−Fe of the bulk deposit, the experimentally obtained critical size of a single domain is reported to be ∼10 nm.[31,32] Spin-polarized STM investigations have revealed single domains of magnetization of Fe islands below a thickness of 6 nm.[33] In the present work, the Fe grains, having a size of 4−6 and 6−7 nm in the pseudorods and pseudosquare rings, respectively, can be considered as single-domain ferromagnetic particles. Second, supported clusters of magnetic metals and alloys have large magnetic exchange length due to intergrain magnetic exchange couplings.[31,32,34] Continuous[35] or incontinuous[31] films composed of spherical Fe grains of 5 nm have been reported to show large magnetization at room temperature. Since the Fe grains in the pseudorods and pseudosquare rings are in contact with each other with very few breaks, strong exchange coupling is expected, which would drive the magnetization of the grains to arrange under magnetostatic constraint, i.e., with maximum magnetostatic interaction. Third, many supported magnetic films[36,37] have been confirmed experimentally to take an in-plane magnetization. Following such a consensus, the easy axis of magnetization of the grains for the pseudorod structure on Au(111) would be along the bcc−Fe[001]

(31) Pierce, J. P.; Torija, M. A.; Gai, Z.; Shi, J.; Schulthess, T. C.; Farnan, G. A.; Wendelken, J. F.; Plummer, E. W.; Shen, J. *Phys. Rev. Lett.* **2004**, *92*, 237201.
(32) Skomski, R. *J. Phys.: Condens. Matter* **2003**, *15*, R841.
(33) Pietzsch, O.; Kubetzka, A.; Bode, M.; Wiesendanger, R. *Science* **2001**, *292*, 2053.
(34) Bansmann, J.; et al. *Surf. Sci. Rep.* **2005**, *56*, 189.
(35) Perez, J. P.; Dupuis, V.; Tuaillon, J.; Perez, A.; Paillard, V.; Melinon, P.; Treilleux, M.; Thomas, L.; Barbara, B.; Bouchet-Fabre, B. *J. Magn. Magn. Mater.* **1995**, *145*, 74.
(36) dos Santos, M. C.; Geshev, J.; Pereira, L. G.; Alves, M. C. M.; Schmidt, J. E.; Allongue, P. *Phys. Rev. B* **2004**, *70*, 104420.
(37) Kawakami, R. K.; Escorcia-Aparicio, E. J.; Qiu, Z. Q. *Phys. Rev. Lett.* **1996**, *77*, 2570.

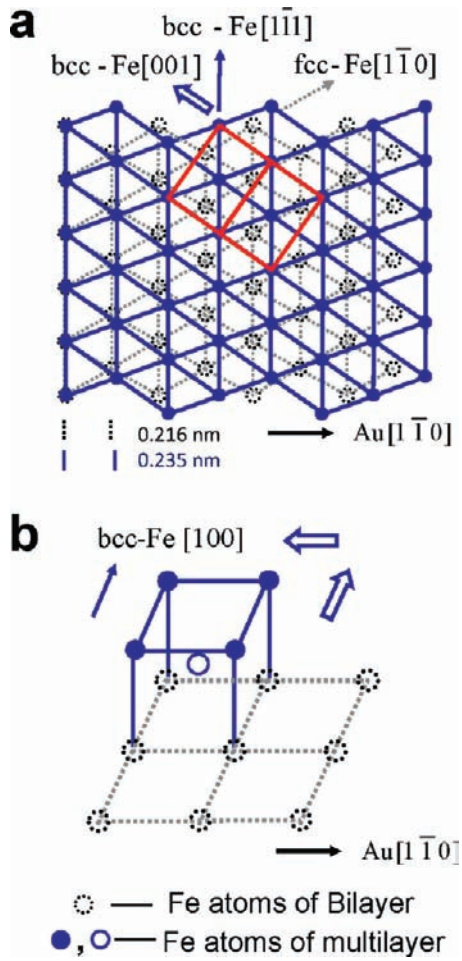

Figure 5. Illustration of lattice planes and magnetic orientations of the 3D pseudorods and pseudosquare rings on the respective bilayers. In (a), the pseudorods lie in bcc−Fe(110) plane (two of its unit cells being highlighted in red) and are oriented along the [1$\bar{1}$1] direction. The easy axis of magnetization along bcc−Fe[001] is rotated from the rod orientation by 54.8°. The bcc−Fe(110) in the multilayer has lattice coincidence with the fcc−Fe(111) bilayer by $0.235 \times 10 \approx 0.216 \times 11 \approx 2.3$ nm along the Au[1$\bar{1}$0] direction. In (b), the pseudosquare rings lie in the bcc−Fe(100) plane and magnetization is along the ⟨100⟩ directions of bcc−Fe crystals, i.e., along the four sides of the square rings. Hollow arrows indicate the magnetic orientations of the Fe grains.

direction, refer to the hollow arrow in Figure 5a. This magnetization is consistent with easy magnetization along ⟨100⟩ directions of usual bcc−Fe bulk crystals, but rotated from the rod orientation in the bcc−Fe[1$\bar{1}$1] direction by 54.8°. For the pseudosquare rings on Au(100), the in-plane magnetization of the grains can be either parallel or perpendicular to the side of the square rings. Both are in easy magnetization directions of usual bulk bcc−Fe in ⟨100⟩ directions, Figure 5b.

Based on the above analysis, we propose a mechanism in Figure 6 based on the magnetic coupling to explain the formation of the shape-ordered Fe structures. For the pseudorod structure on Au(111), antiparallel magnetization of the neighboring grains, both along the surface and between the neighboring layers, would be the magnetostatically stable configurations, Figure 6a, left. With such a configuration the pseudorod structure as a whole would not appear with magnetic poles, except at the joint of the three pseudorods shown in the model. Because of the unfavorable magnetic frustration at the joint, the probability of direct contact between two pseudorods at the end is low in real situation; refer to Figure 3S (Supporting Information).

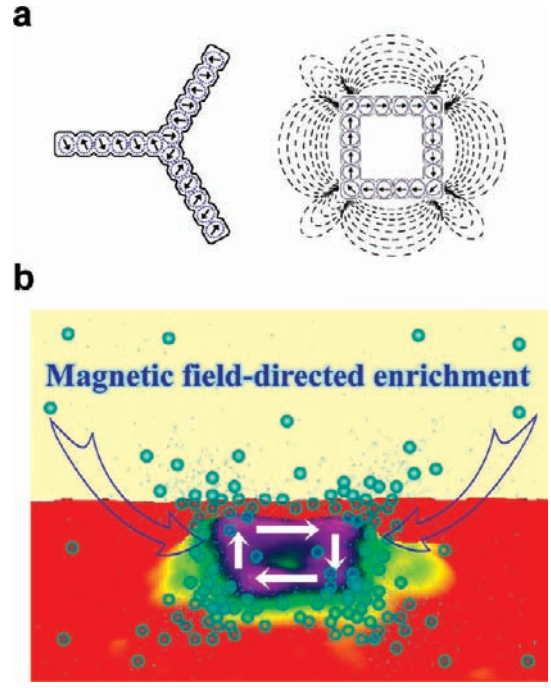

Figure 6. Schematic illustration of magnetization of grains in the pseudorods on Au(111) (a, left) and pseudosquare rings on Au(100) (a, right) and (b) magnetic field-directed enrichment of magnetic reactants. The lower part of (b) is a real STM image of one pseudosquare ring presented in a 3D view in color.

Therefore, the magnetic coupling of the grains on the strips with crystallographic confinement by the surface structure of the substrate may be sufficient to explain the growth of the rodlike structure.

For the pseudosquare rings on Au(100), the unusual ring-type of growth behavior has to be understood by integrating thermodynamic as well as kinetic factors involved in the deposition. The magnetization of the grains along the sides of the ring forms an energetically stable magnetic flux closure, Figure 6a, right. Such a closure creates magnetic poles located at the four corners as well as uncompensated magnetic strength around the outer peripheries of the ring. It is also important to realize that the magnetized Fe nanostructures are small magnets, which would influence the flow of charged species at the vicinity on their way toward the surface. In particular, magnetic reactants such as $FeCl_4^-$ contained in the ionic liquid may be accelerated toward and thus enriched at the magnetic poles of the nanomagnets, which would then alter the local growth kinetics, Figure 6b. The protrusion of the corners of the ring and enlarging "ring-on-ring" growth characteristic would be the results of just such a magnetic field effect. We point out that the coralloid structures formed in the primary stage, though apparently disordered, Figure 3b, have adopted the characteristic structural feature of the Au(100) surface, which enables the crystallographic features of the substrate to be preserved in the follow-up 3D deposition.

The validity of the above discussion of mechanism is based on the assumption that the magnetic coupling among the small Fe grains is sufficiently strong to overcome the influence of thermal energy and orientate their magnetic directions. This is directly related to the size of the Fe grains with respect to the critical size of superparamagnetic limit at room temperature. Cobalt grains of 8 nm have been predicted to be thermally stable

for 10 years.[38] It may be anticipated that the grain size of 4−6 nm in the pseudorods or 6−7 nm in the pseudosquare rings of Fe is just at the boundary approaching the superparamagnetic limit. Here, we consider that the ionic liquid plays an important role in pushing the superparamagnetic limit down to 4−6 nm. Cationic adsorption of ionic liquid at the grains, like a surfactant, may alter the electronic structure of the grains. This surfactant-like effect of the ionic liquid is similar to the thiol-capping effect, which promotes nonferromagnetic Au nanoparticles with 1.4 nm size to show magnetic hysteresis up to room temperature.[39] Again recalling the disordered coralloid film formed at Au(100) in the primary stage, we infer that 4 nm may be a critical size. Below this limit, the magnetostatic interactions among self-magnetized grains would not be sufficient to overcome the thermal energy. The cloudy Fe coralloid structure is likely a result of the lack of sufficient magnetic coupling because of the small grains (2.5−4 nm only). Close inspection of the Ni nanoparticles electrodeposited on Au(111) by Freyland et al.[21] also shows a typical size of the Ni nanoparticles about 5 nm. We believe that magnetization of small ferromagnetic grains in ionic liquids arises from the same origin.

The generality of the growth mechanisms of the pseudorods and pseudosquare rings is verified by formation of essentially the same nanostructures on Pt(111) and Pt(100) surfaces. Pt is also an fcc metal with nearest atomic distance $d_{Pt} = 0.274$ nm. The mismatch of the coincidence lattice of the $2 \times d_{Fe}$ of Fe−fcc (111) and $\sqrt{3} \times d_{Pt}$ of Pt(111) is ∼7%, while the lattice mismatch between the Fe−bcc(100) and Pt(100) planes is ∼4.2%. Both are unfavorable for bilayer epitaxy but small enough to wet the Pt surface. The anisotropy, length and grain size of the pseudorods on Pt(111) and the pseudosquare rings on Pt(100) are consistent with those on the respective Au surfaces, Figure 6S (Supporting Information). It reveals that Fe electrodeposition on fcc metals of Au and Pt follow a common mechanism, and the role of the substrate, regardless of their chemical nature, is to provide an initial crystallographic template which will be developed under the control of magnetic interactions.

It is necessary to point out that the Fe shape-ordered nanostructures have been observed in the absence of external magnetic field, the influence of which on the film morphology deserves a separate investigation. We mention, however, that the pseudosquare rings are formed at sufficiently cathodic potentials, where nucleation and growth is diffusion controlled; refer to Figure 1. Since reactants are more rapidly depleted in the regions around the nuclei, larger concentration gradient and thus larger diffusion flux is expected in these regions, which leads to the *locally inhomogeneous* flow of reactants. It is worth emphasizing that there is a real possibility that the inhomogeneously distributed flux of charged reactants during deposition could induce a local magnetic field that drives the magnetization of the small Fe grains. In fact, such magnetic fields induced by electrochemical reactions have long been observed and investigated for corrosion systems.[40] Since the induced magnetic field in solutions is weak because of the low magnetic susceptibility of the solution medium, its influence on the growth of metal may be negligible, especially in the presence of hydrogen evolution interference. However, this situation might be changed with the use of the more inert ionic liquids with magnetic character, such as the one used in the present work.

4. Summary

In conclusion, we have shown that by employing inert ionic liquid as solvent, not only can the hydrogen evolution interference be avoided, but also the paradigm of nucleation/growth of magnetic metals may be changed. Hitherto unreported shape-ordered structures, namely pseudorods on Au(111) and pseudosquare rings on Au(100) are formed. Magnetostatic interactions under crystallographic constraint and the resultant antiparallel magnetization of the neighboring grains at the pseudorods and magnetic flux closure at the pseudosquare rings are the thermodynamic driving forces for the formation of the respective shape-ordered structures. The uncompensated magnetic field created at the four corners and outer peripheries of the pseudosquare rings further modifies their growth kinetics. Roles of ionic adsorption of the ionic liquid at the electrode surface and the Fe grains as well as local enrichment of magnetic reactant cannot be underestimated. The present work not only opens up a new avenue to form novel magnetic film structures by electrodeposition but also deepens our understanding of magnetism and structure correlation.

Acknowledgment. We are grateful to Prof. J. Y. Kang, Dr. Z. M. Wu, and Prof. D. L. Peng at Xiamen University and to Prof. D. M. Kolb at Ulm University and Prof. M. Blackburn at Sheffield University for reading this manuscript. This work is supported by National Science Foundation of China (Nos. 20673090, 20973141, 20973144, 20911130235, and 50702047).

Supporting Information Available: Complete ref 34, more details, and EC-STM images. This material is available free of charge via the Internet at http://pubs.acs.org.

JA1021816

(38) Welle, D.; Moser, A.; Folks, L.; Best, M. E.; Lee, W.; Toney, M. F.; Schwickert, M.; Thiele, J. U.; Doerner, M. F. *IEEE Trans. Magn.* **2000**, *36*, 10.

(39) Crespo, P.; Litran, R.; Rojas, T. C.; Multigner, M.; de la Fuente, J. M.; Sanchez-Lopez, J. C.; Garcia, M. A.; Hernando, A.; Penades, S.; Fernandez, A. *Phys. Rev. Lett.* **2004**, *93*, 087204.

(40) Juzeliunas, E. *J. Solid State Electrochem.* **2007**, *11*, 791.